



# Study on the Microstructure and Alternating Current Corrosion Behavior of SAF2507 Super-Duplex Stainless Steel in 3.5%NaCl Solution

M. Zhu, Q. Zhang, Y.F. Yuan, S.Y. Guo, and Y.B. Chen

(Submitted June 18, 2019; in revised form January 18, 2020; published online February 6, 2020)

The effect of solution annealing temperature on microstructure and the corresponding AC (alternating current) corrosion behavior was investigated by electrochemical impedance spectroscopy, polarization curve, Mott–Schottky curve and immersion test. With or without AC application, the 2507 SDSS (super-duplex stainless steel) samples annealed at various temperatures exhibit a difference in corrosion resistance. Among them, the corrosion resistance first increases and then decreases as the annealing temperature increases, that is, the 2507 SDSS annealed at 1060 °C has the optimum corrosion resistance, followed by the specimen annealed at 1000 °C, and finally the specimen at 1120 °C. The variation trends of  $R_{ct}$ ,  $R_f$  and  $i_p$  can verify the above law. The  $\sigma$  phase and an excessive amount of  $\alpha$  phase within the microstructure can decrease the corrosion resistance. Additionally, the stability and protective property of passive film formed on the electrode surface is associated with the microstructure of 2507 SDSS. An imposed AC can decrease the passivity of 2507 SDSS and damage the film formed on the sample surface. Furthermore, the corrosion rate and pitting sensitivity of the SDSS increase with the increasing AC current density.

**Keywords** 2507 SDSS, corrosion behavior, imposed AC, microstructure

## 1. Introduction

Duplex stainless steel (DSS) has been widely used in various industries, which is attributed to its excellent combination properties, for example, mechanical property and corrosion resistance (Ref 1-3). In general, the phase ratio of ferrite to austenite and the precipitation of secondary phases are the important factors that can affect the anti-corrosion property (Ref 4-6). Many studies (Ref 7-9) have indicated that DSS samples with approximately equal amounts of ferrite and austenite possess superior corrosion resistance, which is dependent on the chemical composition of constituent phases and appropriate annealing treatments. It is well known that the phase transformation of  $\gamma$ -to- $\alpha$  and the precipitation of intermetallics occur in some temperature ranges (Ref 10, 11), and this change in microstructure can affect the corrosion resistance (Ref 12). Lee et al. (Ref 13) indicated that different solution annealing temperatures affected the surface area ratios of  $\gamma/\alpha$  and critical anodic current densities. Pezzato et al. (Ref 14) investigated the isothermal aging behavior of various DSS samples in the critical temperature range of 750-900 °C. The results showed that secondary phase precipitation mainly influenced the corrosion resistance of lean duplex grades. However, to date, very limited literature has reported the relevance between the annealing temperature and the corrosion

behavior of SAF2507 super-duplex stainless steel. Thus, it is necessary to investigate the above theme.

SAF2507 SDSS is increasingly applied in marine environments due to its outstanding localized corrosion resistance (Ref 15, 16). In this application field, alternating voltage is frequently detected, and some real engineering cases have suggested that the performance degradation of DSS is related to the induction of AC source (Ref 17). Hence, 2507 SDSS, as a structural component, may be easily interfered with by the presence of alternating current (AC). Nevertheless, regarding AC corrosion of 2507 SDSS, no correlative literature has been reported. To date, the research on AC corrosion has mainly focused on pipeline steels, carbon steels, etc. (Ref 18-20). Moreover, these studies mainly involve the mechanism and kinetics of AC-induced corrosion (Ref 21, 22). Unfortunately, there is a lack of reports on the relationship between AC-induced corrosion behavior and the microstructure of 2507 SDSS. Our previous research indicated that the AC corrosion behavior of pipeline steel was closely related to its microstructure (Ref 23). Therefore, it is necessary to investigate the effect of microstructure on AC corrosion behavior of 2507 SDSS in marine environment.

In this work, the corrosion behavior of 2507 SDSS annealed at different temperatures under AC interference is investigated in a simulated seawater solution by several electrochemical measurements and immersion test.

## 2. Experimental

### 2.1 Specimen and Solution

The material used in this paper is a commercial SAF2507 SDSS (UNS S32750). The chemical composition of the stainless steel is (wt.%) C 0.018, Si 0.47, Mn 0.75, P 0.023,

M. Zhu, Q. Zhang, Y.F. Yuan, S.Y. Guo, and Y.B. Chen, School of Mechanical Engineering & Automation, Zhejiang Sci-Tech University, Hangzhou 310018, China. Contact e-mail: zmii2009@163.com.

S 0.001, Cr 25, Ni 6.92, Mo 3.89, N 0.269 and Fe balance. Different annealing temperatures of 1000, 1060 and 1120 °C were applied to manufacture various microstructures with different phase fractions within 2507 SDSS specimens. The specimens (10 × 10 × 5 mm) were annealed at different temperatures for 40 min and subsequently quenched in water. This heat treatment was used to simulate the actual high-temperature applications or the welding procedure found during the fabrication of an engineering structure. Before testing, the oxide film formed on the surface of SDSS samples was thoroughly removed.

The annealed samples were successively ground to 2000 grit SiC abrasive paper, polished with diamond paste to 0.5 μm, degreased with deionized water and alcohol and finally etched in an etchant (20 ml HCl, 80 ml H<sub>2</sub>O and 0.30 g of potassium metabisulfite). Then, the microstructures and chemical compositions of the phases within different annealed samples were analyzed by using scanning electron microscopy (SEM, FEI Quanta 250) and energy-dispersive spectroscopy (EDS). The volume fractions of ferrite (α), austenite (γ) and sigma (σ) phases were measured by quantitative metallography on the stereomicroscope. Each value was the average of at least 10 experimental data.

The experimental solution, 3.5% NaCl with pH value of 7, was prepared by mixing analytically graded sodium chloride and deionized water. The solution temperature was kept constant at 25 °C.

## 2.2 Electrochemical Tests

The annealed specimens were embedded in an epoxy resin, leaving an exposed region of 1 cm<sup>2</sup> as the working surface. Then the steel electrode was sequentially abraded, polished, rinsed and finally dried. In the absence of imposed AC interference, the electrochemical test of the annealed samples was performed using a conventional three-electrode cell via the PARSTAT2273 electrochemical workstation system. The annealed sample was used as a working electrode, a saturated calomel electrode (SCE) as a reference electrode and a platinum sheet as a counter electrode. Firstly, the open circuit potential (OCP) of the samples was recorded for 30 min to reach a stable status. Then, the electrochemical impedance spectroscopy (EIS) measurement was conducted at the open circuit potential in a frequency range from 100 kHz to 10 mHz with the applied disturbance signal amplitude of 10 mV. The potentiodynamic polarization curve was measured at a scanning rate of 0.5 mV/s from −1.2 V (versus SCE) to 1.2 V (versus SCE). Mott–Schottky curve was measured to analyze the difference in the passive films formed on the surface of different annealed samples. The passive film was anodically grown on the samples at an applied potential of 0.8 V (versus SCE) for 1 h. The curves were performed at a fixed frequency of 1 kHz with a 50 mV/step over a potential range from −1.0 to 0.3 V (versus SCE).

Under AC interference, the potentiodynamic polarization curves of the samples annealed at different solution temperatures were tested at various AC current densities of 30, 50 and 100 A/m<sup>2</sup> (the applied AC voltage is 1.25 V). The experimental setup for the electrochemical tests of AC corrosion is in accord with our previous literature (Ref 24, 25). A sinusoidal AC signal wave with 50 Hz frequency was applied between the working electrode of annealed steel and the graphite electrode.

## 2.3 Immersion Test

The specimens were the same as those used in the electrochemical tests, and the superimposed AC circuit in the schematic diagram (Ref 24, 25) was adopted. Prior to testing, the specimen was cleaned, dried and weighed. The test was conducted at the applied AC current density of 100 A/m<sup>2</sup> for 168 h, and the AC signal was applied between the sample and graphite electrode. After the test, the corrosion product covering the sample surface was removed thoroughly. Subsequently, the sample was rinsed, dried and weighed, and then the corrosion rate of the annealed 2507 SDSS was calculated according to the weight loss. The corrosion morphologies and pit initiation sites on the stainless steel samples annealed at different temperatures were observed via SEM. The above tests were repeated at least three measurements.

## 3. Results and Discussion

### 3.1 Microstructure Observation and Analysis

Figure 1 shows the metallographs of 2507 SDSS samples annealed at different temperatures. There is a clear difference among them. Figure 1(a) displays the microstructure of 2507 SDSS annealed at 1000 °C, which consists of darker ferrite (α), lighter austenite (γ) and white σ precipitated phase. Furthermore, the σ phase is granular and short strip, which mainly distributes on the γ and α phases. With the increase in annealing temperature, γ phase evolves from long and thin strip to wide island shape, and the σ phase disappears, as well the grain grows. In addition, for the three annealed microstructures, a small amount of ferrite is distributed within the γ phase.

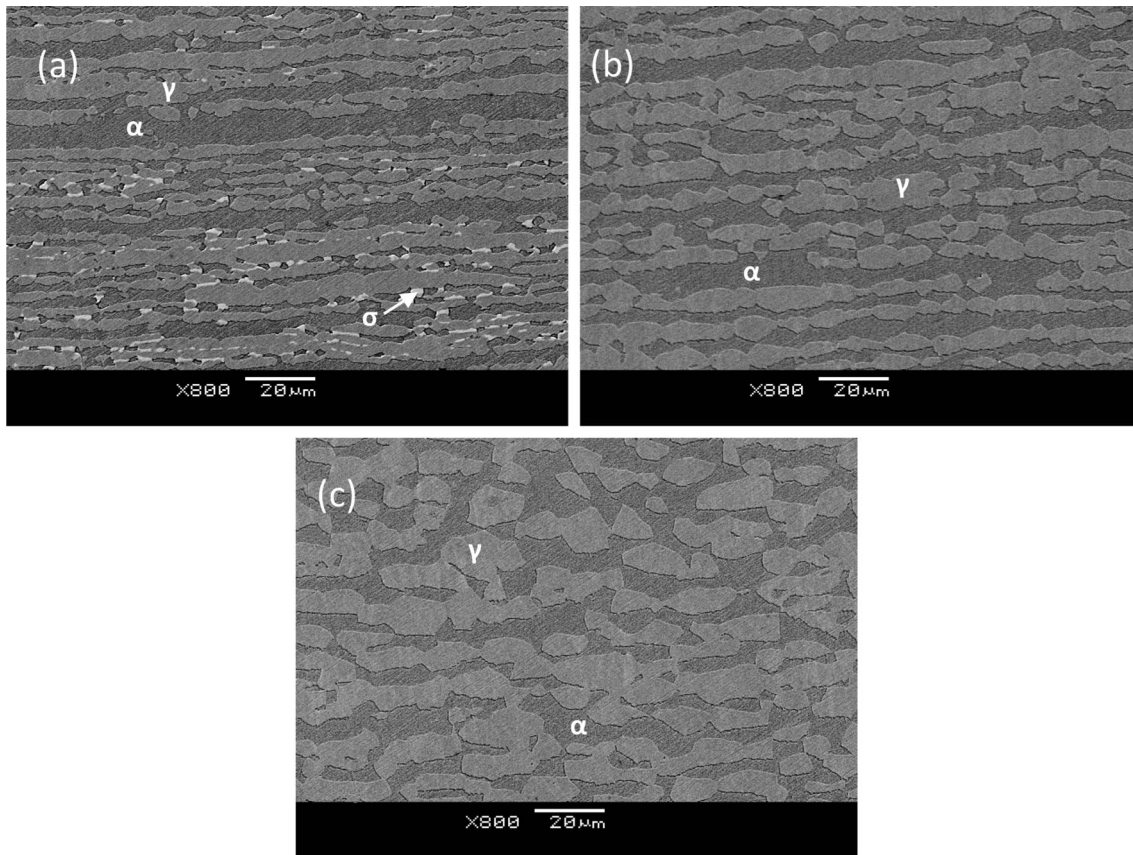
Figure 2 displays the measured phase volume fractions of 2507 SDSS samples annealed at different temperatures. With increasing annealing temperature, the volume fraction of γ phase decreases, whereas that of α phase increases. This may be due to the enhancement of phase transformation of γ → α as the annealing temperature increases, resulting in the decrease in the amount of γ. Moreover, at higher annealing temperatures of 1060 and 1120 °C, no σ phase exists in the microstructure.

The average chemical compositions of main alloying elements in different phases of 2507 SDSS samples annealed at different temperatures are exhibited in Table 1. Compared with γ phase, α phase contains more Cr and Mo elements, while Ni is enriched in γ phase. Additionally, it is clearly seen that Cr and Mo concentrate in σ phase.

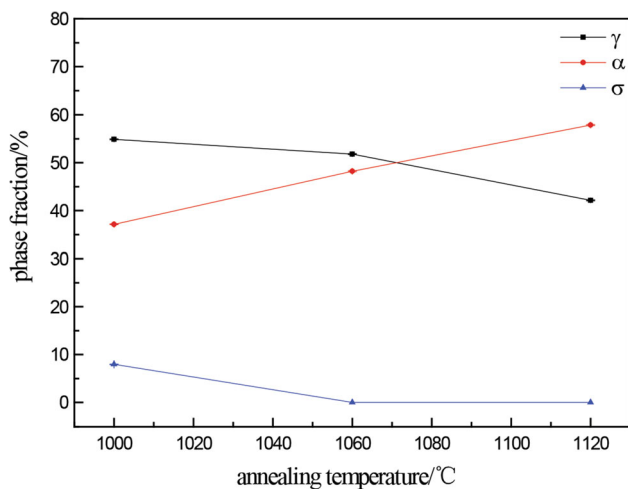
### 3.2 Electrochemical Measurement Without AC Interference

Figure 3 shows the open circuit potential of 2507 SDSS samples annealed at different temperatures. The curves show that the corrosion potential slightly declines with prolonging test time, and finally stabilizes at a relatively stable status. The corrosion potential of specimen annealed at 1060 °C is the most positive, followed by the sample annealed at 1000 °C, and the 2507 SDSS sample annealed at 1120 °C has the most negative corrosion potential value. This suggests that the 2507 SDSS samples annealed at various temperatures have different corrosion tendency.

Figure 4 shows the impedance spectra of 2507 SDSS samples annealed at different temperatures. As revealed in Fig. 4, the curves exhibit the characteristic of capacitive arcs,



**Fig. 1** Metallographs of 2507 SDSS samples annealed at different temperatures (a) 1000 °C; (b) 1060 °C; (c) 1120 °C



**Fig. 2** Phase fraction of 2507 SDSS annealed at different temperatures

with different diameters of impedance semicircles. The sample annealed at 1060 °C has the largest diameter of capacitive loop, followed by that of sample annealed at 1000 °C. This indicates that the 2507 SDSS samples annealed at various temperatures have different anti-corrosion properties. As shown in Fig. 4(b), the Bode plots present two time constants, and the phase angle of impedance measured in the intermediate frequency for the sample annealed at 1120 °C is the lowest. This suggests that the stability of passive film formed on stainless steel annealed at

**Table 1** Average chemical compositions of alloying elements in different phases (wt.%)

Temperature	phase	Cr	Mn	Ni	Mo
1000 °C	σ	26.57	1.21	4.00	9.23
	α	24.32	1.08	4.3	4.46
	γ	23.92	1.04	6.08	3.4
1060 °C	α	24.54	1.04	3.73	5.20
	γ	22.515	1.23	6.63	3.27
1120 °C	α	24.62	1.11	4.02	4.86
	γ	22.32	1.10	6.51	3.13

1120 °C is lower, compared with the other two annealed samples.

The equivalent circuit  $R_s(Q_f R_f)(Q_{dl} R_{ct})$  was used to fit the impedance spectra of 2507 SDSS samples annealed at different temperatures. The circuit assumes (Ref 26, 27) that the passive film was already formed on the surface of stainless steel.  $R_s$  is the solution resistance, and  $Q_f$  represents the capacitance of the passive film, coupled with the resistance of passive film  $R_f$ .  $Q_{dl}$  represents the capacitance of double layer, and  $R_{ct}$  is the charge transfer resistance (Ref 28). In the circuit, constant phase element Q is used for the description of non-ideal capacitance (Ref 29), which replaces the pure capacitance component C attributed to surface heterogeneity (Ref 30).

As listed in Table 2, the stainless steels annealed at various temperatures have different resistance values of passive film  $R_f$ ,

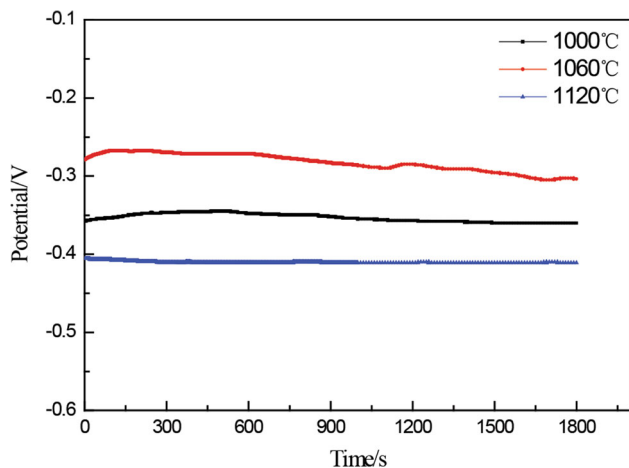


**Fig. 3** Open-circuit potential of 2507 SDSS samples annealed at different temperatures in 3.5% NaCl solution

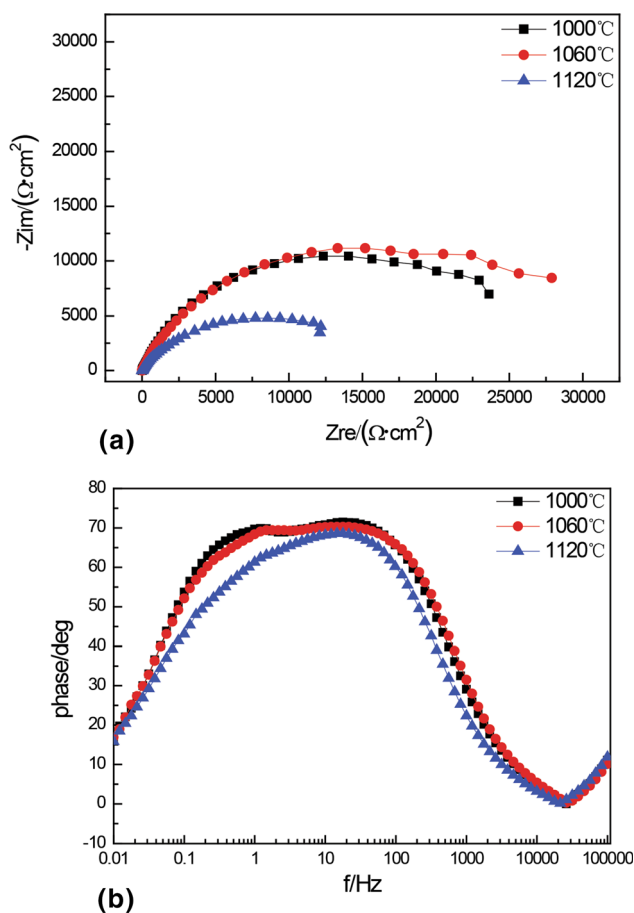


**Fig. 4** Impedance spectra of 2507 SDSS samples annealed at different temperatures (a) Nyquist plot, (b) Bode diagram

indicating that there is a difference in the protective property of passive films formed on the surface of stainless steel samples. Among them, the 2507 SDSS sample annealed at 1060 °C exhibits the maximum  $R_f$  and the minimum value of  $Q_f$ , which suggests that its passive film has the optimum corrosion resistance due to having the fewest amount of defects (Ref 29). Conversely, the film on the stainless steel annealed at 1120 °C

possesses the worst protective property. Moreover, Table 2 reveals that the stainless steel annealed at 1060 °C has the largest  $R_{ct}$  value, followed by 1000 °C, which also reflects that the film on the steel electrode annealed at 1060 °C presents the highest resistance to the charge transfer processes in the base metal/solution interface. The larger the  $R_{ct}$  value, the better the anti-corrosion resistance is (Ref 31). Hence, the 2507 SDSS specimen annealed at 1060 °C has the greatest corrosion resistance, followed by annealing at 1000 °C, and finally annealed at 1120 °C. The difference in corrosion resistance is closely related to the passive film formed on the stainless steel electrode (Fig. 5).

Figure 6 shows the polarization curves of 2507 SDSS samples annealed at different temperatures. The similar anode polarized curves clearly display the obvious characteristics of passivation, which reflects that the samples annealed at various temperatures exhibit the same corrosion kinetics. Moreover, the critical pitting potential values are almost equal. In the cathodic part, there is hardly any difference in the curve shape, while in the anodic branch, an apparent difference in the passive current density is observed. The fitted passive current densities ( $i_p$ ) obtained from the polarization curves of 2507 SDSS samples annealed at different temperatures are 21.25, 20.96 and 24.05  $\mu\text{A cm}^{-2}$  as the annealing temperature increases. In other words, the  $i_p$  value first decreases and then increases. In general, the lower the  $i_p$  value, the lower the corrosion rate is (Ref 28). This means that the stainless steel annealed at 1060 °C possesses the optimal corrosion resistance. This result is in accord with that of EIS test.

In order to further analyze the difference in corrosion resistance of 2507 SDSS annealed at various temperatures, the Mott–Schottky curves were measured.

The Mott–Schottky theory has been applied to investigate the semiconductor properties of passive films on stainless steels (Ref 32, 33). The electrochemical capacitance of the passive film/electrolyte interface is recorded as a function of the applied potential to characterize the semiconductive property. The relationship between the space charge capacitance ( $C$ ) and the applied potential is given by the following Mott–Schottky equation, which describes the applied potential dependence of the capacitance  $C$  for a semiconductor junction under the depletion condition (Ref 34–36) as:

$$C^{-2} = \pm \frac{2}{e\epsilon\epsilon_0 N} \left( E - E_{FB} - \frac{\kappa T}{e} \right) \quad (\text{Eq 1})$$

where the negative sign (–) is for a  $p$ -type semiconductor and the positive sign (+) is for  $n$ -type conductivity,  $e$  is the electron charge ( $1.602 \times 10^{-19}$  C),  $N$  is the donor density ( $N_D$ ) for  $n$ -type or the acceptor density ( $N_A$ ) for  $p$ -type semiconductor.  $\epsilon_0$  is the vacuum permittivity ( $8.854 \times 10^{-14}$  F/cm),  $\epsilon$  is the relative dielectric constant of the passive film.  $k$  is the Boltzmann constant ( $1.38 \times 10^{-23}$  J/K),  $T$  is the absolute temperature (K), and  $\kappa T/e$  is about 25 mV at room temperature.  $E$  is the applied electrode potential and  $E_{FB}$  is the flat band potential. The defect concentration ( $N_D$  or  $N_A$ ) can be calculated from the slope of linear segment in a Mott–Schottky plot ( $C^{-2} - E$ ) (Ref 37).

Figure 7 displays the Mott–Schottky plots of passive films formed on 2507 SDSS samples annealed at different temperatures. In the potential range, all the curves show the negative and positive linear regions, suggesting that the films exhibit the  $p$ -type and  $n$ -type semiconductor behavior. Additionally, the slopes of the curves of 2507 SDSS samples with different

**Table 2** The fitting parameters for the impedance spectra of 2507 SDSS samples

Temperature	$R_s, \Omega \text{ cm}^2$	$Q_f, 10^{-5} \text{ F cm}^{-2}$	$n_1$	$R_f, 10^4 \Omega \text{ cm}^2$	$Q_{dl}, 10^{-5} \text{ F cm}^{-2}$	$n_2$	$R_{ct}, 10^4 \Omega \text{ cm}^2$
1000 °C	9.155	8.841	0.8597	0.2738	4.053	0.8826	2.494
1060 °C	9.028	6.915	0.8882	0.7350	3.644	0.9126	3.118
1120 °C	8.866	14.03	0.8428	0.1962	11.95	0.8981	1.135

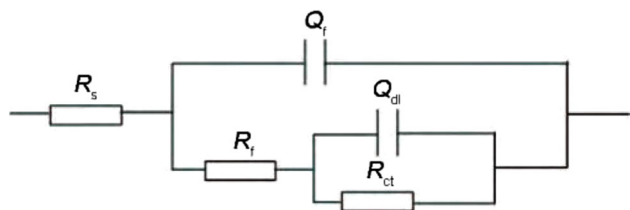


**Fig. 5** Equivalent circuit for fitting EIS diagram

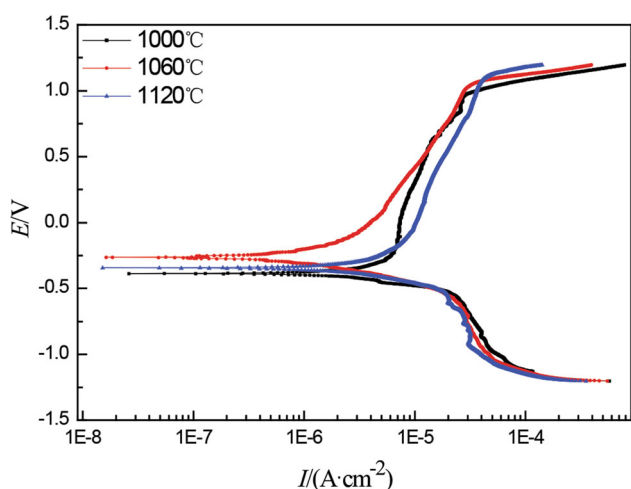


**Fig. 6** Polarization curves of 2507 SDSS samples annealed at different temperatures without AC application

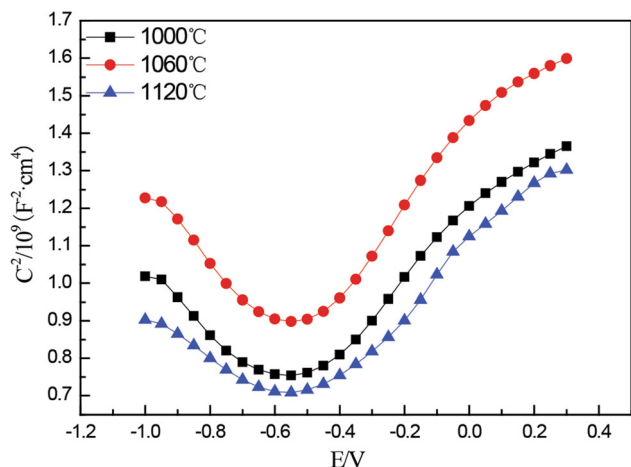


**Fig. 7** Mott-Schottky plots of passive films formed on 2507 SDSS samples annealed at different temperatures

**Table 3** Charge carrier density ( $N_D$  and  $N_A$ ) in the passive films of different 2507 SDSS samples

Annealing temperature, °C	$N_A, 10^{20} \text{ cm}^{-3}$	$N_D, 10^{20} \text{ cm}^{-3}$
1000	9.584	9.799
1060	7.641	6.869
1120	14.147	10.725

annealing temperatures are different, which may be attributed to the difference in the passive film structure. Table 3 shows the calculated charge carrier density ( $N_D$  and  $N_A$ ) in the passive films of different 2507 SDSS samples. Note that the 2507 SDSS sample annealed at 1060 °C presents the minimum values of  $N_D$  and  $N_A$ , revealing a thick passive film with a low conductivity (Ref 38, 39). Furthermore, the corresponding film resistance  $R_f$  is the maximum (Table 2). However, the  $N_D$  and  $N_A$  values of stainless steel sample annealed at 1120 °C are the largest. The donors and acceptors within the semiconducting passive film are defects (Ref 40). This means that the specimen possesses a less stable passive ability, with a thin and highly conductive passive film (Ref 41). Therefore, the structural difference of passive films results in the varying corrosion resistance of 2507 SDSS samples annealed at various temperatures.

### 3.3 Polarization Curve Tested with AC Interference

Figure 8 presents the potentiodynamic polarization curves of 2507 SDSS samples annealed at different temperatures tested under various AC current densities. Compared with the curves measured in the absence of AC application (Fig. 6), the curves tested with imposed AC show an obvious oscillation phenomenon, especially at higher AC current densities of 50 and 100  $\text{A cm}^{-2}$ . With the increasing AC current density, the passive current density ( $i_p$ ) increases, the critical pitting potential shifts negatively, and the passive region gradually narrows. Meanwhile, the distinct active-passive zone can be clearly observed while  $i_{AC}$  is equal to or greater than 50  $\text{A cm}^{-2}$ . This indicates that imposed AC can decrease the passivity of 2507 SDSS, that is, the passivation process becomes difficult, which results in an increase in corrosion rate and pitting sensitivity. Figure 9 displays the fitted  $i_p$  value of different 2507 SDSS samples. The varying values suggest that AC interference accelerates the corrosion of 2507 SDSS as the AC current density increases. In addition, under various  $i_{AC}$ , the stainless steel annealed at 1060 °C has the minimum  $i_p$  value, and the steel specimen annealed at 1120 °C shows the

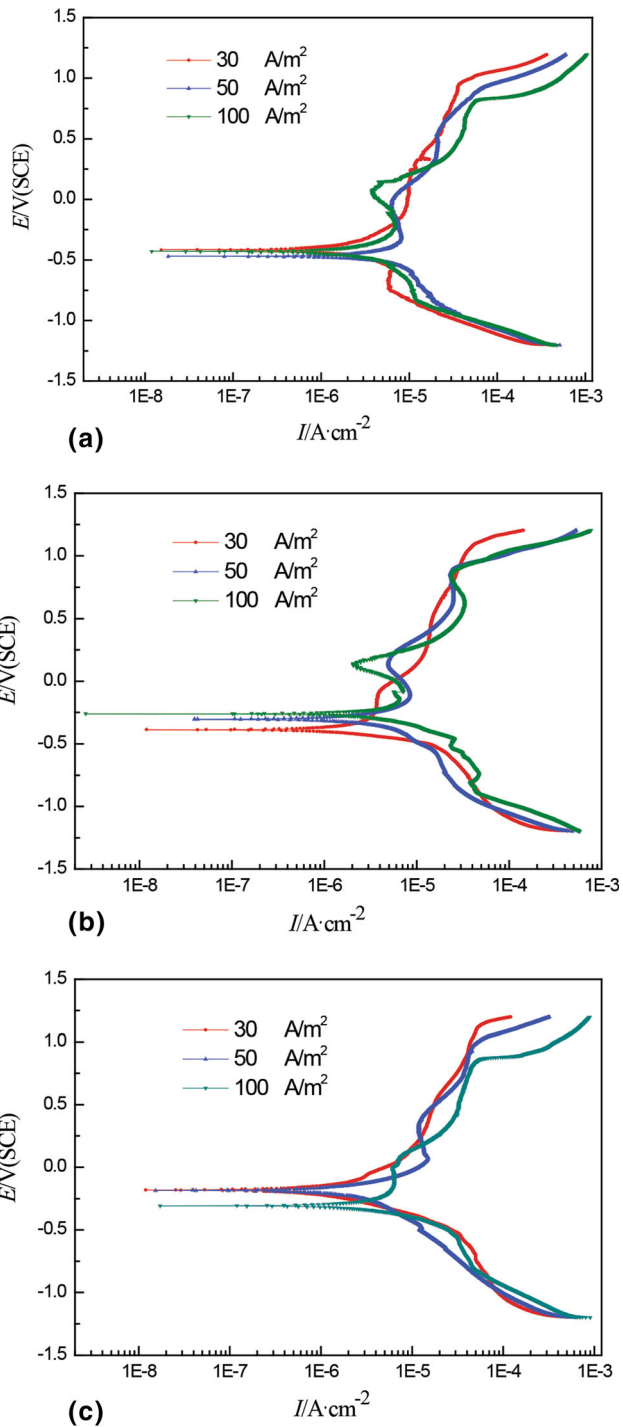


**Fig. 8** Potentiodynamic polarization curves of 2507 SDSS samples annealed at different temperatures tested under various AC current densities (a) 1000 °C; (b) 1060 °C; (c) 1120 °C

maximum value. Thus, the 2507 SDSS samples annealed at different temperatures with AC application possess different corrosion resistance, and the difference becomes more obvious with the increase in  $i_{AC}$ .

### 3.4 Immersion Test

Figure 10 displays the corrosion rates of 2507 SDSS samples annealed at different temperatures under AC interfer-

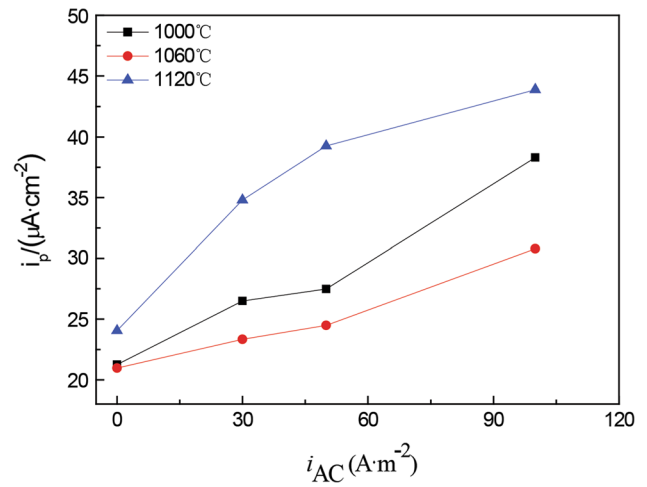


**Fig. 9** Passive current density ( $i_p$ ) of different 2507 SDSS samples at various AC current densities

ence of 100 A/m<sup>2</sup>. The result exhibits that the corrosion rate is reduced first and increased later with the increasing annealing temperature, and the sample annealed at 1060 °C presents the lowest corrosion rate, followed by the sample annealed at 1000 °C, whereas the 2507 SDSS annealed at 1120 °C has the highest value. The result is in accord with that of potentiodynamic curve tested with AC interference.

To further analyze the corrosion behavior of 2507 SDSS specimens with different microstructures under AC application, the distribution of initiation sites for pitting corrosion in the steels annealed at different temperatures was observed. As shown in Fig. 11(a), the pits of sample annealed at 1000 °C are mainly located in the austenite phase, and very few pits are formed in the ferrite phase, which is in agreement with the previous research report (Ref 42). This status of pit initiation is attributed to the lower pitting resistance equivalent number of austenite phase, compared with that of ferrite phase (Ref 42). Hence, preferential corrosion occurs in the austenite phase due to it being the weak phase. Moreover, a clear observation reveals that some pits are distributed in or around the  $\sigma$  phase. This suggests that precipitated  $\sigma$  phase within the microstructure can accelerate the corrosion of 2507 SDSS. Figure 11(b) shows that compared with the other two microstructures, the sample annealed at 1060 °C exhibits the slightest corrosion degree, with rare pitting located at austenite/ferrite boundary. This may be due to the equal proportion of  $\alpha$  and  $\gamma$ , and the grain boundary is served as the pit site because of higher energy and more active. Figure 11(c) reveals the severe corrosion characteristics, with dense pits. The pits occur mostly in austenite phase, and some pits are observed to form in ferrite phase embedded within austenite phase. Moreover, a small number of pits are located at the more dissolved phase side of the phase boundary, i.e., at the  $\gamma$  phase close to  $\alpha$  phase or in an inverse distribution situation. The above results demonstrate that the microstructural difference in 2507 SDSS samples can significantly affect the corrosion resistance. Among them, the constituent phase and its distribution are the crucial factors.

From the above tests, with or without AC application, the 2507 SDSS samples annealed at various temperatures exhibit a difference in corrosion resistance. Among them, the 2507 SDSS annealed at 1060 °C has the optimum corrosion resistance, followed by the specimen annealed at 1000 °C.

That is, the corrosion resistance first increases and then decreases as the annealing temperature increases. This corrosion behavior may be closely related to the microstructure.

For the sample annealed at 1000 °C, the precipitation of  $\sigma$  phase easily causes the deficiency of Cr and Mo contents in the area around  $\sigma$  phase. This is attributed to the high amounts of Cr and Mo in  $\sigma$  phase. Thus, the difference in the electrochemical activity leads to the formation of local corrosion cells, which can accelerate the occurrence of corrosion, resulting in that the pits can occur near the sigma phase due to the local

reduction of chromium and other elements. With the increase in annealing temperature, the phase ratio of ferrite and austenite is approximately about 1:1, without the presence of  $\sigma$  phase. The microstructure is beneficial for improving corrosion resistance, and many researches demonstrate this (Ref 5, 43). However, for 2507 SDSS sample annealed at 1120 °C, the phase fraction of ferrite is much greater than that of austenite (Fig. 2). The increase in the amount of ferrite as the weak phase (Ref 44, 45) reduces the corrosion resistance. Many researchers (Ref 46) found that as the annealing temperature increases, the ferrite phase is more susceptible to corrosive attack. This is attributed to the change in chemical composition of ferrite phase.

Furthermore, the results of EIS test, polarization curve and Mott-Schottky plot indicate that there are differences that exist in the protective property of passive films formed on the surface of stainless steels annealed at various temperatures, which would affect the corrosion resistance of 2507 SDSS samples. The sample annealed at 1060 °C has the maximum film resistance  $R_f$ , the minimum defect amount ( $N_D$  and  $N_A$ ), and the lowest passive current density ( $i_p$ ), which means that a more stable and better protective passive film is formed on the sample surface. In contrast, the film on the sample annealed at 1120 °C possesses the worst protective ability. Essentially, the difference is associated with the microstructure of 2507 SDSS sample. Zhang et al. (Ref 47) also reported that the changes in the phase proportion of the microstructure and the distribution of the alloying elements caused by solution annealing treatment did not change the semiconductor type of the passive films formed on the DSS surface, but affected the density of defects

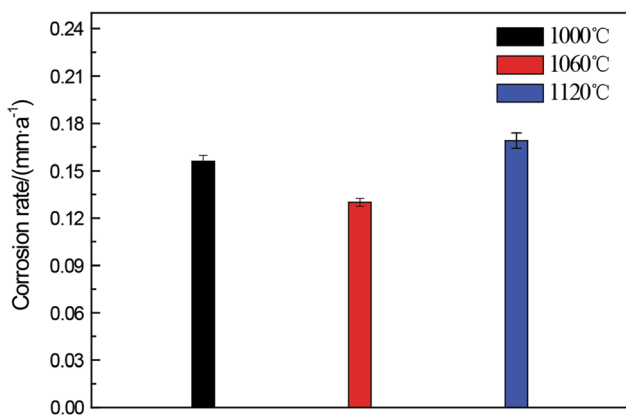


**Fig. 10** Corrosion rates of 2507 SDSS samples annealed at different temperatures under AC interference

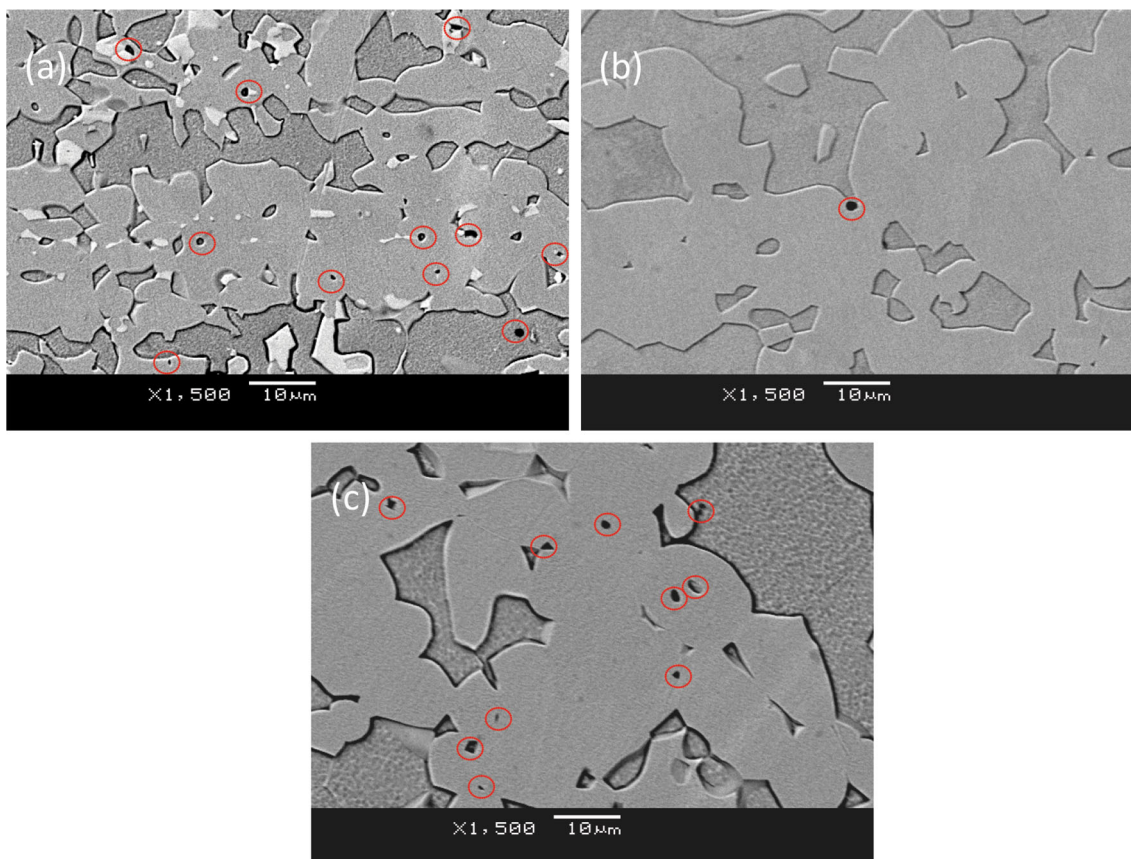


**Fig. 11** Occurrence position of pits on 2507 SDSS samples annealed at different temperatures under AC interference (a) 1000 °C; (b) 1060 °C; (c) 1120 °C

and the stability of the passive film, that is, the corrosion resistance.

In the presence of superimposed AC, the passivity and stability of the passive film become even worse, especially at a high AC current density of 100 A/m<sup>2</sup>. This is due to the fact that the applied AC can prevent the formation of passive film and damage the film formed on the steel surface (Ref 41). The higher the AC current density, the greater the destructive effect is. This suggests that the number of channels for the penetration and transfer of ions, molecules and charges increase. The unstable and broken film cannot effectively inhibit the solution infiltrating into the metal interface, resulting in the rapid occurrence of electrochemical corrosion and pit initiation.

## 4. Conclusions

With or without AC application, 2507 SDSS samples annealed at various temperatures exhibit the difference in corrosion resistance. Among them, the corrosion resistance first increases and then decreases as the annealing temperature increases, that is, the 2507 SDSS annealed at 1060 °C has the optimum corrosion resistance, followed by the specimen annealed at 1000 °C, and finally the specimen at 1120 °C. The corrosion behavior may be closely related to the microstructure.  $\sigma$  phase and an excessive amount of  $\alpha$  phase within the microstructure can decrease the corrosion resistance. Additionally, the stability and protective property of passive film formed on the electrode surface are associated with the microstructure of 2507 SDSS sample.

Imposed AC can decrease the passivity of 2507 SDSS samples and damage the film formed on the sample surface. Furthermore, the corrosion rate and pitting sensitivity increase as the AC current density increases.

## Acknowledgments

This work was supported by the National Natural Science Foundation of China, the Natural Science Foundation of Zhejiang province (No. LY18E010004) and the National R&D Infrastructure and Facility Development Program of China (No. 2005DKA10400).

## References

1. Z.Y. Zhang, H. Zhao, H.Z. Zhang, J. Hu, and J.R. Jin, Microstructure Evolution and Pitting Corrosion Behavior of UNS32750 Super Duplex Stainless Steel Welds After Short-Time Heat Treatment, *Corros. Sci.*, 2017, **121**, p 22–31
2. N. Ebrahimi, M. Momeni, M.H. Moayed, and A. Davoodi, Correlation Between Critical Pitting Temperature and Degree of Sensitisation on Alloy 2205 Duplex Stainless Steel, *Corros. Sci.*, 2011, **53**, p 637–644
3. V. Vignal, D. Ba, H. Zhang, F. Herbst, and S. Le Manchet, Influence of the Grain Orientation Spread on the Pitting Corrosion Resistance of Duplex Stainless Steels Using Electron Backscatter Diffraction and Critical Pitting Temperature Test at the Microscale, *Corros. Sci.*, 2013, **68**, p 275–278
4. J.K.L. Lai, K.W. Wong, and D.J. Li, Effect of Solution Treatment on the Transformation Behaviour of Cold-Rolled Duplex Stainless Steels, *Mater. Sci. Eng. A Struct.*, 1995, **A203**, p 356–364
5. H.Y. Ha, M.H. Jang, T.H. Lee, and J. Moon, Interpretation of the Relation Between Fraction and Pitting Corrosion Resistance of Commercial 2205 Duplex Stainless Steel, *Corros. Sci.*, 2014, **89**, p 154–162
6. L.Q. Guo, M. Li, X.L. Shi, Y. Yan, X.Y. Li, and L.J. Qiao, Effect of Annealing Temperature on the Corrosion Behavior of Duplex stainless Steel Studied by in Situ Techniques, *Corros. Sci.*, 2011, **53**, p 3733–3741
7. D.H. Kang and H.W. Lee, Study of the Correlation between Pitting Corrosion and the Component Ratio of the Dual Phase in Duplex Stainless Steel Welds, *Corros. Sci.*, 2013, **74**, p 396–407
8. S.T. Kim, I.S. Lee, J.S. Kim, S.H. Jang, Y.S. Park, K.T. Kim, and Y.S. Kim, Investigation of the Localized Corrosion Associated with Phase Transformation of Tube-to-Tube Sheet Welds of Hyper Duplex Stainless Steel in Acidified Chloride Environments, *Corros. Sci.*, 2012, **64**, p 164–173
9. H. Tan, Z.Y. Wang, Y.M. Jiang, D. Han, J.F. Hong, L.D. Chen, L.Z. Jiang, and J. Li, Annealing Temperature Effect on the Pitting Corrosion Resistance of Plasma Arc Welded Joints of Duplex Stainless Steel UNS S32304 in 1.0 M NaCl, *Corros. Sci.*, 2011, **53**, p 2191–2200
10. R.A. Perren and T. Suter, Corrosion Resistance of Super Duplex Stainless Steels in Chloride Ion Containing Environments: Investigations by Means a New Microelectrochemical Method: II. Influence of Precipitates, *Corros. Sci.*, 2001, **43**, p 727–745
11. E. Angelini and B. De Benedetti, Microstructural Evolution and Localized Corrosion Resistance of an Aged Super Duplex Stainless Steel, *Corros. Sci.*, 2004, **46**, p 1351–1367
12. N. Lopez, M. Cid, and M. Puiggali, Influence of  $\sigma$ -phase on mechanical properties and corrosion resistance of duplex stainless steels, *Corros. Sci.*, 1999, **41**, p 1615–1631
13. J.S. Lee, S.H. Jeon, and Y.S. Park, Effects of Solution Annealing Temperature on the Galvanic Corrosion Behavior of the Super Duplex Stainless Steels, *J. Mater. Eng. Perform.*, 2013, **22**, p 557–562
14. L. Pezzato, M. Lago, K. Brunelli, M. Breda, and I. Calliari, Effect of the Heat Treatment on the Corrosion Resistance of Duplex Stainless Steels, *J. Mater. Eng. Perform.*, 2018, **27**, p 3859–3868
15. J.M. Pardal and S.S.M. Tavares, Effect of the Heat Treatment on the Corrosion Resistance of Duplex Stainless Steels, *Mater. Charact.*, 2009, **60**, p 165–172
16. J.C. Lacerda, L.C. Cândido, and L.B. Godefroid, Effect of Volume Fraction of Phases and Precipitates on the Mechanical Behavior of UNS S31803 Duplex Stainless Steel, *Int. J. Fatigue*, 2015, **74**, p 81–87
17. L. Sjogren, G. Camitz, J. Peultier, S. Jacques, V. Baudu, F. Barrau, B. Chareyre, A. Bergquist, A. Pourbaix, and P. Carpentiers, Corrosion Resistance of Stainless Steel Pipes in Soil, *Mater. Corros.*, 2011, **62**, p 299–309
18. D. Kuang and Y.F. Cheng, Understand the AC Induced Pitting Corrosion on Pipelines in Both High pH and Neutral pH Carbonate/Bicarbonate Solutions, *Corros. Sci.*, 2014, **85**, p 304–310
19. S.B. Lalvani and G. Zhang, The Corrosion of Carbon Steel in A Chloride Environment Due to Periodic Voltage Modulation: Part I, *Corros. Sci.*, 1995, **37**, p 1567–1582
20. H.X. Wan, D.D. Song, C.W. Du, Z.Y. Liu, and X.G. Li, Effect of Alternating Current and Bacillus Cereus on the Stress Corrosion Behavior and Mechanism of X80 Steel in a Beijing Soil Solution, *Bioelectrochemistry*, 2019, **127**, p 49–58
21. S.B. Lalvani and X. Lin, A Revised Model for Predicting Corrosion of Materials Induced by Alternating Voltages, *Corros. Sci.*, 1996, **38**, p 1709–1719
22. R.W. Bosch and W.F. Bogaerts, A Theoretical Study of AC-Induced Corrosion Considering Diffusion Phenomena, *Corros. Sci.*, 1998, **40**, p 323–336
23. M. Zhu, Y.F. Yuan, S.M. Yin, G.H. Yu, S.Y. Guo, Y.Z. Huang, and C.W. Du, Corrosion Behavior of Pipeline Steel with Different Microstructures Under AC Interference in Acid Soil Simulation Solution, *J. Mater. Eng. Perform.*, 2019, **28**, p 1698–1706
24. M. Zhu, C.W. Du, X.G. Li, Z.Y. Liu, H. Li, and D.W. Zhang, Effect of AC on Stress Corrosion Cracking Behavior and Mechanism of X80 Pipeline Steel in Carbonate/Bicarbonate Solution, *Corros. Sci.*, 2014, **87**, p 224–232
25. M. Zhu, C.W. Du, X.G. Li, Z.Y. Liu, S.R. Wang, J.K. Li, and D.W. Zhang, Effect of AC Current Density on Stress Corrosion Cracking Behavior of X80 Pipeline Steel in High pH Carbonate/Bicarbonate Solution, *Electrochim. Acta*, 2014, **117**, p 351–359



26. A. Kocijan, D.K. Merl, and M. Jenko, The Corrosion Behaviour of Austenitic and Duplex Stainless Steels in Artificial Saliva with the Addition of Fluoride, *Corros. Sci.*, 2011, **53**, p 776–783
27. H. Luo, C.F. Dong, X.G. Li, and K. Xiao, The Electrochemical Behaviour of 2205 Duplex Stainless Steel in Alkaline Solutions with Different pH in the Presence of Chloride, *Electrochim. Acta*, 2012, **64**, p 211–220
28. L. Freire, M.J. Carmezima, and M.G.S. Ferreira, The Electrochemical Behaviour of Stainless Steel AISI, 304 in Alkaline Solutions with Different pH in the Presence of Chlorides, *Electrochim. Acta*, 2011, **56**, p 5280–5289
29. H. Luo, H.Z. Su, C.F. Dong, and X.G. Li, Passivation and Electrochemical Behavior of 316L Stainless Steel in Chlorinated Simulated Concrete Pore Solution, *Appl. Surf. Sci.*, 2017, **400**, p 38–48
30. K. Jüttner, Electrochemical Impedance Spectroscopy (EIS) of Corrosion Processes on Inhomogeneous Surfaces, *Electrochim. Acta*, 1990, **35**, p 1501–1508
31. C.N. Cao, *Principles of Electrochemistry of Corrosion*, 3rd ed., Chemical Industry Press, Beijing, 2008
32. A. Fattah-Alhosseini, F. Soltani, F. Shirsalimi, B. Ezadi, and N. Attarzadeh, The Semiconducting Properties of Passive Films Formed on AISI, 316 L and AISI, 321 Stainless Steels: A Test of the Point Defect Model (PDM), *Corros. Sci.*, 2011, **53**, p 3186–3192
33. Y.C. Zhang, M.U. Macdonald, G.R. Engelhardt, and D.D. Macdonald, Development of Localized Corrosion Damage on Low Pressure Turbine Disks and Blades: I. Passivity, *Electrochim. Acta*, 2012, **69**, p 1–11
34. F. Mao, C. Dong, S. Sharifi-Asl, P. Lu, and D.D. Macdonald, Macdonald, Passivity Breakdown on Copper: Influence of Chloride Ion, *Electrochim. Acta*, 2014, **144**, p 391–399
35. V.A. Alves and C.M.A. Brett, Characterization of Passive Films Formed on Mild Steels in Bicarbonate Solution by EIS, *Electrochim. Acta*, 2002, **47**, p 2081–2091
36. J. Sikora, E. Sikora, and D.D. Macdonald, Electronic Structure of the Passive Film on Tungsten, *Electrochim. Acta*, 2000, **45**, p 1875–1883
37. A. Goossens, M. Vazquez, and D.D. Macdonald, The Nature of Electronic States in Anodic Zirconium Oxide Films Part 1: The Potential Distribution, *Electrochim. Acta*, 1996, **41**, p 35–45
38. H.C. Tian, X.Q. Cheng, Y. Wang, C.F. Dong, and X.G. Li, Effect of Mo on Interaction between  $\alpha$  /  $\gamma$  Phases of Duplex Stainless Steel, *Electrochim. Acta*, 2018, **267**, p 255–268
39. Z.Y. Cui, S.S. Chen, Y.P. Dou, S. Han, L.W. Wang, C. Man, X. Wang, S.G. Chen, Y.F. Cheng, and X.G. Li, Passivation Behavior and Surface Chemistry of 2507 Super Duplex Stainless Steel in Artificial Seawater: Influence of Dissolved Oxygen and pH, *Corros. Sci.*, 2019, **150**, p 218–234
40. C. Sunseri, S. Piazza, and F. Quarto, Photocurrent Spectroscopic Investigations of Passive Films on Chromium, *J. Electrochem. Soc.*, 1990, **137**, p 2411–2417
41. M. Zhu and C.W. Du, A New Understanding on AC Corrosion of Pipeline Steel in Alkaline Environment, *J. Mater. Eng. Perform.*, 2017, **26**, p 221–228
42. H. Tan, Y.M. Jiang, B. Deng, T. Sun, J.L. Xu, and J. Li, Effect of Annealing Temperature on the Pitting Corrosion Resistance of Super Duplex Stainless Steel UNS S32750, *Mater. Charact.*, 2009, **60**, p 1049–1054
43. H.Y. Ha, M.H. Jang, T.H. Lee, and J. Moon, Understanding the Relation between Phase Fraction and Pitting Corrosion Resistance of UNS S32750 Stainless Steel, *Mater. Charact.*, 2015, **106**, p 338–345
44. Z. Zhang, Z. Wang, Y. Jiang, H. Tan, D. Han, Y. Guo, and J. Li, Effect of Post-Weld Heat Treatment on Microstructure Evolution and Pitting Corrosion Behavior of UNS S31803 Duplex Stainless Steel Welds, *Corros. Sci.*, 2012, **62**, p 42–50
45. Z. Zhang, H. Zhao, H. Zhang, Z. Yu, J. Hu, L. He, and J. Li, Effect of Isothermal Aging on the Pitting Corrosion Resistance of UNS S82441 Duplex Stainless Steel Based on Electrochemical Detection, *Corros. Sci.*, 2015, **93**, p 120–125
46. M.A. Domínguez-Aguilar and R.C. Newman, Detection of Deleterious Phases in Duplex Stainless Steel by Weak Galvanostatic Polarization in Alkaline Solution, *Corros. Sci.*, 2006, **48**, p 2560–2576
47. J.T. Zhang, X.J. Hu, P. Lin, and K.C. Chou, Effect of Solution Annealing on the Microstructure Evolution and Corrosion Behavior of 2205 Duplex Stainless Steel, *Mater. Corros.*, 2018, **70**, p 676–687

**Publisher's Note** Springer Nature remains neutral with regard to jurisdictional claims in published maps and institutional affiliations.